Cofactor Activation and Substrate Binding in Pyruvate Decarboxylase. Insights into the Reaction Mechanism from Molecular Dynamics Simulations†

Mette Alstrup Lie,‡ Leyla Celik,§ Karl Anker Jørgensen,‡ and Birgit Schiøtt*,§

Danish National Research Foundation, Center for Catalysis, and the Department of Chemistry, Aarhus University, DK-8000 Aarhus C, Denmark

Received June 14, 2005; Revised Manuscript Received September 15, 2005

ABSTRACT: We have performed long-term molecular dynamics simulations of pyruvate decarboxylase from *Zymomonas mobilis*. Nine structures were modeled to investigate mechanistic questions related to binding of the cofactor, thiamin diphosphate (ThDP), and the substrate in the active site. The simulations reveal that the proposed three ThDP-tautomers all can bind in the active site and indicate that the equilibrium is shifted toward 4′-aminopyrimidine ThDP in the absence of substrate. 4′-Aminopyrimidinium ThDP is found to be a likely intermediate in the equilibrium. Mutations of important active site residues, Glu473Ala and Glu50Ala, were modeled to further elucidate their catalytic role. Formation of the catalytic important ylide by deprotonation of ThDP(C2) is investigated. Only the less favored tautomer, 1′,4′-iminopyrimidine ThDP (imino-ThDP), could be deprotonated. The two other tautomers of ThDP could not be activated at the C2-position, thus, explaining the mechanistic importance of the less stable imino-ThDP. Finally, binding of pyruvate in the active site with the cofactor modeled as the nucleophilic ylide (ylide-ThDP) is studied. The carbonyl group of the substrate forms a hydrogen bond to Tyr290(OH). No hydrogen bond could be identified between ThDP(N4′) and the substrate. The geometry of the substrate binding is well-suited for a nucleophilic attack by ylide-ThDP(C2). We propose that a proton relay from His113 via Asp27 and Tyr290 to the carbonyl oxygen atom of the substrate may be involved in the mechanism.

Thiamin diphosphate (ThDP),[1] the biological active form of vitamin B1, is an essential cofactor for a number of enzymes in the carbohydrate metabolism, where it is involved in the decarboxylation of α-keto acids. Pyruvate decarboxylase (PDC) catalyzes the first step in ethanol fermentation, converting pyruvate to acetaldehyde (eq 1) (*1*).

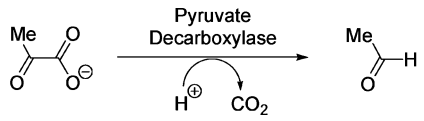

(1)

Vitamin B1 was discovered in the 1930s (*2*, *3*); however, its physiological function was almost unknown at that time. ThDP consists of a diphosphate group and two aromatic rings, a pyrimidine and a thiazolium ring, bridged by a methylene group; see Scheme 1. It was demonstrated in the 1950s that thiamin itself can catalyze reactions such as those catalyzed by PDC (*4*). Breslow showed that the catalytic active form of ThDP is an ylide (ylide-ThDP), produced by deprotonation of ThDP(C2) of the thiazolium ring (see Scheme 1 for atom numbering) (*5*). Ylide-ThDP then attacks the carbonyl group of pyruvate leading to formation of C2α-lactyl-ThDP (lactyl-ThDP). The thiazolium ring of ThDP acts after decarboxylation as an electron sink leading to the formation of a resonance-stabilized enamine. Addition of a proton gives C2α-hydroxyethyl-ThDP (hydroxyethyl-ThDP), followed by regeneration of the ylide-ThDP by release of acetaldehyde (*6*). The originally proposed mechanism left much uncertainty about formation of the catalytic active ylide and the role of the pyrimidine ring (*3*, *7*).

ThDP-dependent enzymes have recently attracted attention in organic synthetic chemistry. They have been used as catalysts in chemoenzymatic syntheses performing regio- and enantioselective reactions (*8*, *9*). PDC has been shown to function as a carboligase in the synthesis of chiral α-hydroxy ketones. The reverse reaction of PDC, incorporation of CO_2 into acetaldehyde, has also been demonstrated (*10*).

In the 1990s, several high-resolution X-ray structures provided additional insight into the machinery of ThDP-dependent enzymes (*11*−*13*). ThDP is bound to the enzyme through three conserved hydrogen bonds (Figure 1). Mg(II) ions also assist in anchoring ThDP to the protein by forming an octahedral coordination sphere.

In the active site of all ThDP-dependent enzymes, ThDP is bound in a *V*-conformation (*11*−*13*) with the consequence

† This work was supported by the Danish Natural Science Foundation and the Danish National Research Foundation.

* To whom correspondence should be addressed. E-mail, birgit@chem.au.dk; fax, +45 8619 6199; phone, +45 8942 3953.

‡ Danish National Research Foundation, Center for Catalysis.

§ Department of Chemistry, Aarhus University.

[1] Abbreviations: ThDP, thiamin diphosphate; PDC, pyruvate decarboxylase; ylide-ThDP, C2-deprotonated ylide from ThDP; lactyl-ThDP, C2α-lactyl-ThDP, the pyruvate-ThDP adduct; hydroxyethyl-ThDP, C2α-hydroxyethyl-ThDP, the acetaldehyde-ThDP adduct; ZmPDC, pyruvate decarboxylase from *Zymomonas mobilis*; YPDC, pyruvate decarboxylase from yeast; amino-ThDP, 4′-aminopyrimidine tautomer of ThDP; imino-ThDP, 1′,4′-iminopyrimidine tautomer of ThDP; pyrimidinium-ThDP, 4′-aminopyrimidinium form of ThDP; CD, circular dichroism; MD, molecular dynamics; SBMD, stochastic boundary molecular dynamics; RESP, restrained eletrostatic potential; SD, steepest descent; ABNR, adopted basis Newton−Raphson; NAC, near-attack conformation; rmsd, root-mean-square deviation; QM/MM, quantum mechanics/molecular mechanics.

10.1021/bi051134y CCC: $30.25
Published on Web 10/22/2005

Scheme 1: Reaction Mechanism of ThDP-Dependent Enzymes[a]

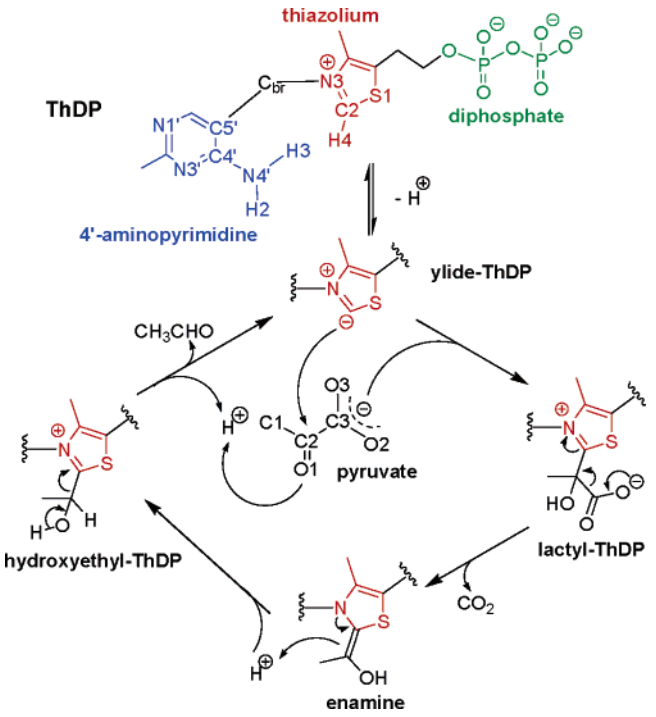

[a] Atom labeling is shown.

that the N4′-nitrogen and C2-carbon atoms of ThDP are in close proximity. Experimental findings support that both the N1′-nitrogen atom and the exocyclic N4′-amino group of the pyrimidine ring are essential for activation of the cofactor (*14*). N1′-Methylthiamin model studies by Jordan et al. revealed that the catalytic active ylide is generated by an intramolecular proton transfer from C2 to N4′ (*13a*, *14b*). Kern et al. have shown that the interaction between the conserved Glu50 and the N1′-nitrogen atom of ThDP activates the N4′-amino group for functioning as a proton acceptor toward the C2-proton, as they observed a reduced rate constant for deprotonation of C2 by either mutation of Glu50 or by elimination of the N1′- or N4′-nitrogen atom of ThDP (*14h*). On the other hand, Washabaugh et al. have proposed that a general base in the active site can be responsible for deprotonation of ThDP(C2) and that neither the N4′-amino group nor the interaction between Glu50 and ThDP(N1′) contributes significantly to the activation of ThDP (*15*).

Tautomerization and proton-transfer reactions play very crucial roles in many chemical and biochemical reaction mechanisms (*16*). Due to the physical nature of the interaction of X-rays with molecules, hydrogen atoms are hard to identify correctly from X-ray diffraction experiments. Therefore, experimental methods of choice have often been from more indirect spectroscopic evidence (*17*) with NMR emerging as a strong alternative (*18*). Focus has been on understanding the environmental effects on tautomeric equilibria, steric factors, electronic factors, as well as geometric constraints (*19*). For ThDP-dependent enzymes, it has been proposed that a tautomeric equilibrium between 4′-aminopyrimidine (amino-ThDP) and 1′,4′-iminopyrimidine ThDP (imino-ThDP) is important for the reaction. The tautomeric equlibrium has been proposed to be catalyzed by an interaction between Glu50 and ThDP(N1′) and possibly to proceed through an intermediate 4′-aminopyrimidinium tautomer (pyrimidinium-ThDP); see Scheme 2 (*14*). Experimental studies led Jordan et al. to propose that the function of the conserved residue Glu473 might be to deprotonate pyrimidinium-ThDP(N4′), forming the rare imino-ThDP, and that the catalytic active ylide is generated from imino-ThDP (*12*, *14a*). This proposal has received further support by experimental results from circular dichroism (CD) spectroscopy of imino-ThDP (*20*). The positive charge imposed on the pyrimidine ring in pyrimidinium-ThDP is supposed to initiate the conversion of the N4′-amino group, which is a very weak acid, into an N4′-imino group, being a weak base. Potential general bases nearby ThDP(N4′) that could abstract

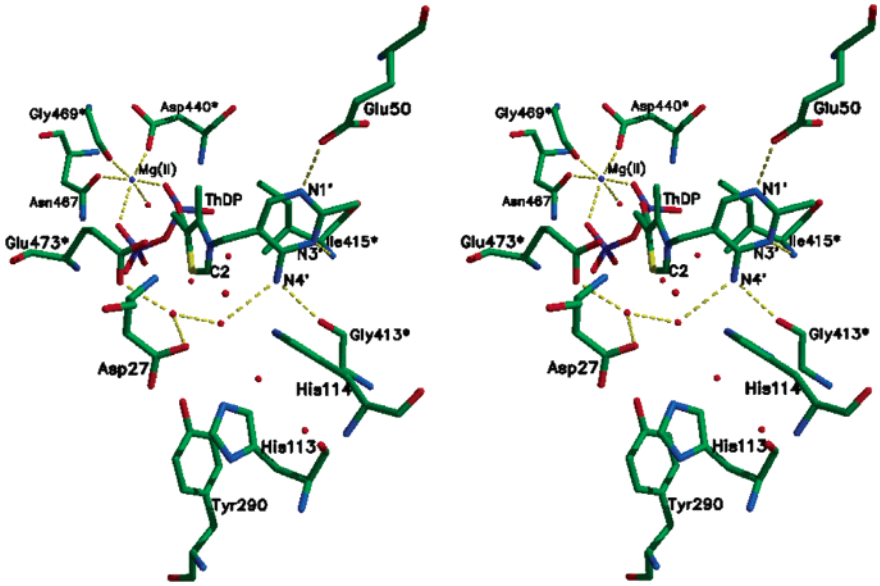

FIGURE 1: Active site in the X-ray crystal structure of PDC from *Zymomonas mobilis* (ZmPDC) (*11*). ThDP from yeast PDC (*12*) (YPDC) has been substituted for the cofactor analogue found in ZmPDC (see Modeling of the Cofactor and Pyruvate). Residues from the C-terminal of one monomer are marked by a star; no star denotes residues from the N-terminal of the other monomer in the tight dimer. The stars are omitted in the figures throughout the rest of the paper. Crystal waters are shown as red dots. *Zymomonas mobilis* numbering is used throughout the paper.

Scheme 2: Tautomeric Equilibrium and Ylide Generation in ThDP-Dependent Enzymes

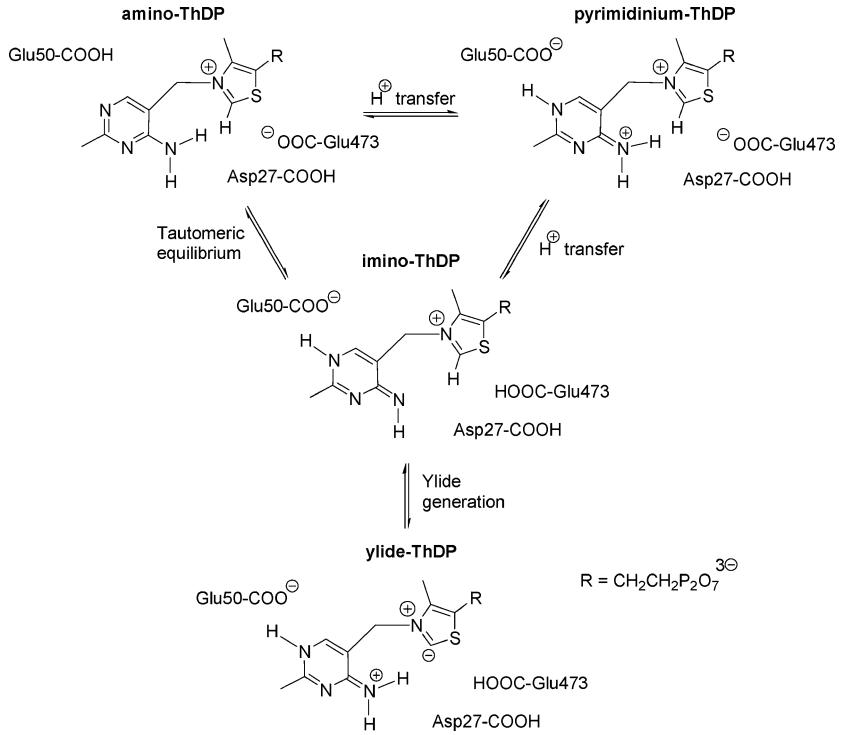

the N4′-proton from pyrimidinium-ThDP are Asp27, Glu473, His114, and His113. Site-directed mutagenesis studies on YPDC have shown that the mutant Asp27Ala is 7-fold less active than the wild-type and that the YPDC mutant Glu473Asp shows less than 2% activity (*21*). A mutagenesis study on the ZmPDC mutant His113Gln shows complete loss of activity (*22*). These results imply a catalytic function of these residues.

A few modeling studies of ThDP-dependent enzymes have appeared. Lobell and Crout studied the proposed mechanism for YPDC with focus on the decarboxylation steps (*23*). Simple minimizations of each intermediate of the mechanism were reported, allowing adducts of ThDP (excluding the diphosphate), substrate, water molecules, and three active side residues to move. Friedemann et al. have performed molecular dynamics (MD) simulations on YPDC (*24*). They studied the isolated cofactor and a few analogues, as well as the cofactor bound in the protein. However, their short 0.5 ns simulations did only include a limited fraction of the protein. Focus was on the conformational behavior of ThDP and on the presence of a hydrogen bond between Glu50 and ThDP(N1′). Thus, these studies investigated neither activation of ThDP nor substrate binding. Friedemann et al. have also performed DFT studies of some later steps in ThDP-dependent catalysis (*25*), but never including solvent effects, apo-enzymatic effects, or the imino tautomer of ThDP (*25*).

In this paper, we present long-term MD simulations of ZmPDC that include a very large part of the enzymatic environment and all three tautomers of ThDP. The results help disentangle the activation of ThDP by examing the stability of the three ThDP tautomers. MD simulations have recently proven to be a useful tool in studying hydrogen transfer reactions (*26*) and is a well-suited method for studying the tautomeric equilibria of ThDP in the enzymatic active site as well as the formation of ylide-ThDP. Finally, binding and orientation of the substrate, pyruvate, in the active site, is analyzed, and a reaction pathway for the nucleophilic attack is proposed.

MATERIALS AND METHODS

General Setup. To the best of our knowledge, ZmPDC is the only PDC that shows simple Michaelis−Menten kinetics (*27*). All other pyruvate decarboxylases show a sigmoidal dependence of reaction velocity on substrate concentration, implying substrate activation for the allosteric enzyme (*28*). Therefore, to be certain to use an active structure as the starting structure for the simulations, the crystal structure from ZmPDC is used (*11*). Stochastic boundary molecular dynamics (SBMD) simulations (*29*) were performed on ZmPDC with cofactor ThDP in the active sites using the program CHARMM (*30*), version 27b4, and the CHARMM27 all-atom force field parameters (*31*). Force field parameters for imino-type nitrogen atom in the ThDP tautomers were generated from similar tautomers of nucleic acids (*32*).

A total of nine active sites are modeled (Table 1). The first three models contain the three tautomers of the pyrimidine ring of ThDP. The next three models are included for studying the effect of mutations of important amino acids in the active site (*14a*, *14h*, *21*). Models **7** and **8** examine the protonation states of active site residues Asp27 and Glu473. Two water molecules are placed at the substrate binding site in models **1**−**8**. To investigate the orientation of pyruvate in the active site and the first step in the catalytic cycle, model **9** contains ylide-ThDP at the ThDP binding site and pyruvate at the substrate binding site.

Modeling of the Cofactor and Pyruvate. The X-ray crystal structure of ZmPDC (pdb code 1ZPD) was downloaded from the Protein Data Bank (*33*) and was used as starting structure for all simulations (*11*). The structure contains 4 × 565 amino acids, four partially degraded analogues of ThDP instead of the intact cofactor, four Mg(II) ions, four citrate

Table 1: The Nine Active Site Models Simulated in the Present MD Study[a]

active site model	ThDP tautomer	Glu50	Glu473	Asp27	substrate binding site
1	amino-ThDP	protonated	deprotonated	protonated	two waters
2	pyrimidinium-ThDP	deprotonated	deprotonated	protonated	two waters
3	imino-ThDP	deprotonated	protonated	protonated	two waters
4	amino-ThDP	mutated to Ala and two waters	deprotonated	protonated	two waters
5	pyrimidinium-ThDP	deprotonated	mutated to Ala and two waters	protonated	two waters
6	pyrimidinium-ThDP	deprotonated	mutated to Ala and two waters	deprotonated	two waters
7	amino-ThDP	protonated	protonated	deprotonated	two waters
8	pyrimidinium-ThDP	deprotonated	protonated	deprotonated	two waters
9	ylide-ThDP	deprotonated	protonated	protonated	pyruvate

[a] Protonation states of catalytic important residues and molecules occupying the substrate binding site are listed.

molecules, and 2569 water molecules. For construction of the catalytic active enzyme complex, the four cocrystallized chemically incomplete cofactors found in 1ZPD were deleted. Four cofactors, from the crystal structure of YPDC (*12*) (PDB code 1PVD), were docked into the active sites by matching four atoms using MidasPlus (*34*) (Figure S2 in Supporting Information).

ThDP has several titratable groups and can therefore exist as different tautomers, amino-, imino- and pyrimidinium-ThDP (Scheme 2). These tautomers differ in the number and distribution of protons on the nitrogen atoms N1′ and N4′. ThDP, as found in the X-ray crystal structure 1PVD (*12*), has been used as a scaffold for modeling all ThDP derivatives. In model **9**, pyruvate was docked into the active site by matching the position of the oxygen atoms in the two cocrystallized water molecules found at the substrate binding site in 1ZPD with pyruvate(O1) and pyruvate(O2) (see Scheme 1 for numbering), respectively, as proposed by Dobritzsch et al. (*11*). The partial atomic charges of the ThDP tautomers were obtained by quantum chemical calculations using Gaussian98 (*35*). The electrostatic potentials were calculated using the Merz−Singh−Kollman procedure (*36*) by fitting atomic point charges to the electrostatic potential derived from the electron density, calculated at the HF/6-31 +*G*(*d*) level of theory (*37*). To fit the charges to the electrostatic potential and to give equivalent atoms identical charges, the restrained electrostatic potential method (RESP) was then used (*38*). The same procedure was used to obtain the partial atomic charges of ylide-ThDP, citrate ion, and pyruvate. As there are no standard parameters in the CHARMM27 force field describing neither the cofactor as either of the tautomers, nor ylide-ThDP, citrate ion, nor pyruvate, Accelrys-CHARMm parameters, as included in the program Quanta 2000 (*39*), were used to model these structures accordingly, together with parameters developed for similar nucleic acids tautomers (*32*). The computed partial charges, the added values for force constants, and van der Waals terms are tabulated in the Supporting Information.

Amino Acid Protonation States. Hydrogen atoms were added to the X-ray coordinates of the enzyme and crystal water molecules using the H-build facility in CHARMM. The protonation state of all histidines were evaluated based on the availability of proximal hydrogen bond donors and acceptors and are listed in the Supporting Information. On the basis of experimental evidence, His113 and His114 are modeled protonated and unprotonated, respectively (*11*). The protonation states of the catalytic important residues Asp27, Glu50, and Glu473 are listed in Table 1 for each of the models and are further described in the Supporting Information. All other aspartate, glutamate, arginine, and lysine residues were modeled charged, and all tyrosine residues were kept neutral.

Minimization. The resulting structures have overall sizes of approximately 85 × 100 × 120 Å^3 and contain approximately 42 000 atoms, including 2569 crystal water molecules. The potential energy of each system was minimized using a combination of two minimization steps: 500 steps of steepest descent (SD) followed by 10 000 steps (or until convergence has been met) of adopted-basis Newton−Raphson (ABNR). The crystal coordinates were initially subjected to this two-step minimization with all non-hydrogen atoms fixed. The minimized structures were then subjected to a second round of the two-step minimization with all non-hydrogen atoms constrained by weak harmonic constraints (1 kcal/(mol·Å^2)).

Stochastic Boundary Molecular Dynamics Simulations. For SBMD, each system was divided into a reaction region, a buffer region, and a reservoir region (*29*). As the atom Leu51(CB) of chain F is closest to the midpoint between the most distal atoms of the two cofactors in one of the tight dimers, it was used as the reference point for partitioning of the system. The reaction region is a sphere with a radius of 33 Å centered at the reference point, and it includes two active sites. The spherical buffer region is 2 Å thick, and occupies the space between 33 and 35 Å from the reference point. The reservoir region corresponds to distances larger than 35 Å from the reference point. The shortest distance from a cofactor atom to the reservoir region is ∼15 Å in this setup, which is adequate for modeling the interactions in the system. The system was solvated in an equilibrated TIP3P (*40*) water sphere of 37 Å radius using the defined origo. Any solvent molecule within 2.8 Å of a heavy atom of the enzyme or crystallographic water molecule was deleted. A re-solvation procedure was then performed four times to avoid cavities in the solvation sphere.

To speed up the computational process, all atoms further away than 50 Å from the reference point were deleted after the minimization. The resulting systems consisted of approximately 31 000 atoms, including ∼2800 water molecules. To prevent water from evaporating from the solvent surface, a spherical boundary potential was applied (*29*). During dynamics, the atoms in the reservoir region were frozen. All atoms in the reaction region were treated by the ordinary equations of motion, using Verlet leapfrog dynamics (*41*). A gradual change in forces was inserted by use of the buffer region. All buffer region atoms were treated as interacting

Langevin atoms (*29*, *42*). The heavy atoms of the enzyme in the buffer region were constrained using force constants $m_i\Omega_i^2 = 3k_BT/\langle\Delta r^2\rangle$, where the average root-mean square fluctuations were calculated from their average Debye−Waller *B*-factors (*11*): $\langle\Delta r^2\rangle^{1/2} = (3B/8\pi^2)^{1/2}$ (*43*). Additionally, the buffer region atoms were coupled to a heat bath of 300 K with a frictional coefficient of 250 ps^{-1} on the heavy-protein atoms (*29*). The frictional coefficient of buffer region water oxygen atoms was assigned to 124 ps^{-1}. All force and friction coefficients were scaled throughout the buffer region so that they are zero at the boundary between the reaction region and the buffer region and scaled by 0.5 at the buffer region reservoir region boundary. The SBMD simulations were thus carried out as outlined by Brooks et al. (*29*), with the exception that the force coefficients on the water oxygen atoms were scaled throughout the buffer region, similarly to the protein atoms. To reduce computation time, the Coulombic terms were cutoff at 13 Å by use of a force-shifting function, and a switching function was used for the van der Waals energy between 10 and 11 Å (*44*). An integration step of 1 fs was used. The nonbonded list was updated every 20 time steps, and coordinates were saved every 100 time steps. The SHAKE algorithm was applied to all covalent bonds involving hydrogen atoms, by constraining to the equilibrium distances (tolerance 10^{-6}) (*45*). All simulations were carried out to 2 ns.

Structural Analysis. Trajectories of reaction region residues after the initial 500 ps of equilibration were considered for analysis; thus, 15 000 MD structures, collected during the time period of 500−2000 ps, were averaged for analysis for each of the nine models. Positional fluctuations around the average structure were calculated for the backbone C_α-atoms and compared to those obtained from the crystal structure *B*-factors. The trajectories from each of the MD simulations were analyzed using the concept of Near Attack Conformations (NAC) (*46*). All transformations studied involve proton transfers. The geometric criterion for NAC formation in a proton relay is based on ideal conditions for hydrogen bonds. The transition of making bonds begins upon entering van der Waals interaction, so a NAC is a ground-state conformation where overlap of the van der Waals spheres has just begun. The distance criteria in the present MD simulations have been chosen such that the distances between bond-forming atoms must be equal to or less than the sum (*46a*) of their van der Waals radii (*47*). For simplicity, no lower limits for the distances have been used. Angles corresponding to a proton transfer, as defined by the hydrogen donor, the hydrogen atom, and the hydrogen acceptor, must be close to linear. A deviation of 30° is accepted in this study (*48*). Structural visualization of the enzyme complexes was carried out using the program gOpenMol (*49*). The molecular figures were drawn using Chimera (*50*) or MidasPlus (*34*).

RESULTS AND DISCUSSION

Stability of the MD Simulations. The root-mean-square fluctuation of the temperature for each of the simulations was less than 5 K; thus, the differences observed in the dynamics cannot be ascribed to instabilities in the simulation protocol. As a measure of structural stability, the root-mean-square deviation (rmsd) as a function of simulation time was calculated. The rmsd values were calculated by least-squares fitting of the positions of the Cα-atoms in the reaction region to the positions in the minimized structure. The picture is the same for all simulations: after an initial increase during the equilibration period for the first 500 ps, a plateau of ∼0.75 Å is reached, thus, indicating a stable and equilibrated protein complex. Figures are included in the Supporting Information.

The positional fluctuations of the Cα-atoms in the reaction region were calculated from the full 2.0 ns MD trajectories and compared to those calculated from the Debye−Waller *B*-factors of the crystal structure by use of the equation $\langle\Delta r^2\rangle^{1/2} = (3B/8\pi^2)^{1/2}$ (*43*, *51*). Plots of the positional fluctuations are included in the Supporting Information. The positional fluctuations from the simulation show very good consistency with the positional fluctuations derived from the experimental *B*-factors (*11*). Some residues give higher fluctuations in the simulation than found in the crystal. These residues are all found to be solvent-exposed in the simulations and are therefore expected to show more motion than in the crystal where they can be constrained due to packing effects. Overall, based on the calculated rmsd values as a function of simulation time and on the positional fluctuations for the sampled structures for all simulations, we believe that the local motions sampled in the MD trajectories are reasonable and thus that the nine 2.0 ns simulations for PDC represent a realistic picture of the dynamics of the enzyme when complexed to the cofactor ThDP.

Binding of ThDP. Hydrogen bonds to all three of the nitrogen atoms of the pyrimidine ring, Figure 1, have been proposed from all X-ray structures reported (*11*−*13*, *28*). A realistic and reliable MD simulation will be in agreement with the experimentally determined X-ray structures by revealing conserved hydrogen bonds throughout the simulation. Table 2 lists the distances of these hydrogen bonds, averaged for the four active sites in the crystal structure of ZmPDC (*11*) in the first row, averaged for the two active sites from the crystal structure of YPDC (*12*) in the second row, and, for models **1**−**9**, averaged during the production dynamics, in the remaining rows. From Table 2, it appears that the heteroatomic donor−acceptor distances measured from the X-ray crystal structures are in nice quantitative agreement with those obtained from the MD simulations and that all hydrogen bonds are computed to be close to linear.

The distance between ThDP(N3′) and Ile415(N) varies from 3.19 to 3.78 Å in models **1**−**9** and is thereby loose, in agreement with X-ray structures (*11*−*13*). The hydrogen bonds to N1′ and N4′ appear to be stronger, with heteroatomic distances of approximately 2.7 and 2.8 Å, respectively. The existence of these highly conserved hydrogen bonds throughout the simulation is yet another indication of the reliability of the sampled MD trajectories. The diphosphate side chains interact throughout the simulations with the protein: directly through hydrogen bonds, indirectly through water mediated hydrogen bonds, and through coordination to the second cofactor, the Mg(II) ion. In each of the models, the octahedral coordination of Mg(II) is unaltered during the simulation.

The relative orientation of the pyrimidine and thiazolium rings can be described by the torsional angles Φ_T = C2−N3−C_{br}−C5′ and Φ_P = N3−C_{br}−C5′−C4′ (C_{br} is the bridging methylene carbon atom) as defined by Pletcher and Sax (*52*). *V*-conformations, which are defined by (Φ_P, Φ_T) = (±90°, ∓90°), are formed exclusively for all nine models

Table 2: Nonbonded Distances (Å) and Hydrogen Bond Angles (deg) for the Three Conserved Hydrogen Bonds to the Pyrimidine Ring of X-ray Structures and the MD Averaged Structures (500−2000 ps)[a]

active site model	tautomer of ThDP	ThDP(N1′)···Glu50(OE2) (Å)	∠ThDP(N1′)-ThDP(H1)···Glu50(OE2) (deg)	ThDP(N3′)···Ile415(N) (Å)	∠ThDP(N3′)···Ile415(HN)-Ile415(N) (deg)	ThDP(N4′)···Gly413(O) (Å)	∠ThDP(N4′)-ThDP(H2) ···Gly413(O) (deg)	improper dihedral of N4′ (deg)
ZmPDC (*11*)[b]		2.58	NA	3.19	NA	2.80	NA	NA
YPDC (*12*)[c]		2.67	NA	3.13	NA	2.70	NA	NA
1	amino-ThDP	2.74 ± 0.10	162.0 ± 8.5	3.19 ± 0.18	160.6 ± 8.1	2.77 ± 0.11	156.5 ± 9.8	26.7 ± 9.4
2	pyrimidinium-ThDP	2.77 ± 0.12	166.2 ± 7.4	3.78 ± 0.24	158.9 ± 11.0	2.79 ± 0.12	162.8 ± 8.1	0.7 ± 3.3
3	imino-ThDP	2.72 ± 0.11	159.0 ± 11.5	3.55 ± 0.27	160.2 ± 8.2	2.85 ± 0.13	157.4 ± 9.4	NA
4	amino-ThDP[d]	NA	NA	3.31 ± 0.21	160.1 ± 8.0	2.76 ± 0.10	160.9 ± 9.2	28.7 ± 9.0
5	pyrimidinium-ThDP[e]	2.76 ± 0.12	165.5 ± 8.0	3.52 ± 0.26	158.7 ± 9.9	2.76 ± 0.11	159.1 ± 9.4	0.9 ± 3.4
6	pyrimidinium-ThDP[f]	2.73 ± 0.10	160.7 ± 9.0	3.21 ± 0.19	161.5 ± 8.7	2.83 ± 0.13	154.1 ± 10.1	1.0 ± 3.3
7	amino-ThDP[g]	2.77 ± 0.13	163.7 ± 7.8	3.27 ± 0.18	158.5 ± 9.7	2.78 ± 0.11	156.7 ± 9.3	29.7 ± 9.0
8	pyrimidinium-ThDP[g]	2.76 ± 0.02	162.5 ± 8.0	3.37 ± 0.20	160.3 ± 8.3	2.77 ± 0.11	160.5 ± 9.0	1.4 ± 3.4
9	ylide-ThDP	2.77 ± 0.14	159.0 ± 11.6	3.34 ± 0.20	159.3 ± 8.0	2.79 ± 0.11	164.2 ± 8.3	0.3 ± 3.3

[a] Standard deviations are included. Some properties are not available (NA). [b] Average of four active sites. [c] Average of two active sites. [d] Mutant apoenzyme: Glu50Ala. [e] Mutant apoenzyme: Glu473Ala; Asp27-COOH. [f] Mutant apoenzyme: Glu473Ala; Asp27-COO^-. [g] Reversed protonation: Asp27-COO^-, Glu473-COOH.

simulated, as can be seen from their (Φ_P,Φ_T)-plots in the Supporting Information. The findings of *V*-conformations as being the stable conformation in the MD simulations are in accordance with X-ray crystal structural data (*11*−*13*) and the short time MD simulations by Friedemann et al. *(24)*. The improper dihedral angle for ThDP(N4′) can be used as a measure of the planarity of the ThDP(N4′) amino group, with a value of 0° denoting a planar arrangement around the N4′-nitrogen atom. Values for this improper dihedral are included in the last column in Table 2. The observed planarity of the N4′-amino group in model **2** indicates a favorable resonance between the aromatic pyrimidinium ring and the N4′-nitrogen lone pair in pyrimidinium-ThDP. This is in agreement with experimental NMR studies by Jordan et al. (*14b*, *14d*). Planarity of the N4′-amino group is not observed for amino-ThDP in either model **1**, **4**, or **7**, indicating limited resonance between the aromatic ring and the amino group in this tautomer. However, throughout the MD simulation, no rotation is observed around the ThDP(C4′)−ThDP(N4′) bond in the amino-ThDP models, although a free pyramidal N4′-amino group is expected to rotate (*14d*). In that way, the proton ThDP(H3) (see Scheme 1) keeps pointing toward the thiazolium ring, and ThDP(H2) is consistently hydrogen-bonded to the backbone oxygen atom of Gly413 with an average distance of 1.84 ± 0.13 Å. This conserved hydrogen bond is likely to be the reason for the observed restricted rotation of the exocyclic 4′-amino group, when ThDP is enzyme-bound. Thus, to the extent experimental data exists, the MD results reproduce the experiments, which makes us further believe that the force field-based models are adequate for studying the finer details of the binding of ThDP in PDC. Furthermore, the MD findings of a planar N4′-group in pyrimidinium-ThDP and the observed deviation from planarity in amino-ThDP are in agreement with a DFT study by Friedemann et al. (*25a*).

Tautomeric Equilibrium: Formation of Imino-ThDP. X-ray diffraction methods are not ideal for locating hydrogen atoms. Therefore, the high-resolution structures of PDC do not provide definite evidence as of which tautomer of ThDP is present. MD simulations have shown to be a suitable tool for studying tautomers and proton transfers (*26*). Because MD uses a classical description of the atoms in a system, the topology of the system is unchanged throughout an MD simulation, and as a consequence, no bond making or breaking event can be simulated directly. However, through a careful comparative analysis of the MD trajectories obtained by studying the different tautomers, it is possible to gain knowledge of the most likely active site topology. To do this, we analyzed the conformations sampled during production dynamics for formation of ground state structures that geometrically must be formed prior to reaching the transition state of the reaction studied, for example, for NACs (*46*).

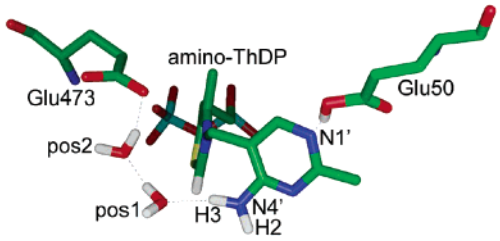

FIGURE 2: Shapshot of a NAC for the proton relays from the conserved Glu50 to amino-ThDP(N1′) and from amino-ThDP(N4′) to the conserved Glu473 in model **1**, transforming the former into imino-ThDP directly. Water molecules are included at pos1 and pos2. Only polar hydrogens are shown for clarity.

Generation of imino-ThDP from amino-ThDP involves two proton relays: one from Glu50(OE2) to ThDP(N1′) and another from ThDP(N4′) to a base in the active site. According to recent CD experiments, this has been suggested to be Glu473(OE2) (*14a*, *20*); see Scheme 2. Model **1** is a proper setup for addressing this proposed transformation. The heteroatomic distance between ThDP(N4′) and Glu473(OE2) is 5.90 Å in the crystal structure of ZmPDC (*11*); thus, the primary role of the conserved residue Glu473 will not be to deprotonate the N4′-amino group by a *direct* transfer. A proton relay pathway from ThDP(N4′) to Glu473 with the intermediacy of two water molecules seems possible based on a detailed inspection of the sampled MD trajectories. The proton relay from ThDP(N4′) to Glu473(OE2) is expected to be a concerted transfer of three protons, as indicated in Figure 2: the first from ThDP(N4′) to a water molecule located at the position labeled pos1, the second from the water molecule at pos1 to another water molecule located at position 2, pos2, and the third transfer from this water molecule at pos2 to Glu473(OE2). On the basis of acidity

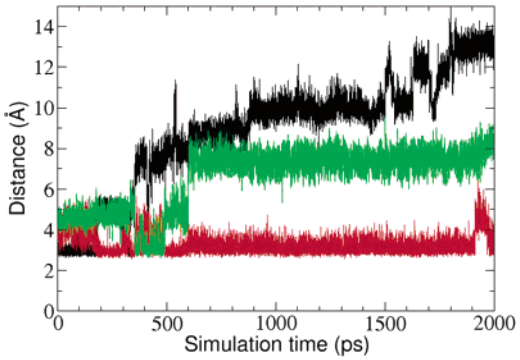

FIGURE 3: Time-dependent variation of separations of the amino-ThDP(N4′) and the oxygen atoms of different crystal water molecules in model **1**. The distance from ThDP(N4′) to xwat603-(O) is displayed in black, to xwat226(O) in red, and to xwat274-(O) in green.

arguments, we do not believe the proton relay to happen stepwise, but rather as a concerted process. For carbonic anhydrase, similar computations have revealed that at proton transfer via a similar "proton wire" with two water molecules is indeed concerted (*53*).

We now want to address whether the water molecules occupying pos1 and pos2 are correctly oriented for relaying the proton from ThDP(N4′) to Glu473(OE2). It appears from Figure 3 that the water molecule xwat603 is positioned in hydrogen-bond distance to ThDP(N4′) at the beginning of the simulation and until approximately 190 ps. At that time, xwat603 leaves the active site and water molecule xwat226 enters the active site. During the time period from 370 to 490 ps, water molecule xwat274 replaces water xwat226, and in the time period from 1920 to 1970 ps, no water molecule could be identified in hydrogen-bond distance to ThDP(N4′). As production dynamics corresponds to the time period of 500−2000 ps, water molecule xwat226 occupies pos1 of Figure 2 for most of the simulation.

The water molecule located at pos2 in Figure 2 is identified as crystal water molecule xwat384 throughout the simulation. The heteroatomic distances between ThDP(N4′) and the waters occupying pos1 and pos2 are almost unaltered during the simulation. Also, it appears from Figure 3 that pos1 constitutes a mobile water environment, which can be speculated as being where the substrate initially enters the active site by first exchanging with this water molecule. A proton relay from ThDP(N4′) to Glu473 is thus present with respect to the heteroatomic distances. However, to do the NAC calculation, the protons must be taken into account. Figure 2 shows a NAC for this proton relay with a simultaneous protonation of N1′, thereby converting amino-ThDP to imino-ThDP in a single step. A NAC for this transformation is defined by the four indicated distances in Figure 2 and the corresponding four angles; 2219 out of the 15 000 sampled structures in model **1** are identified as NACs, corresponding to 15%, indicating that the direct transition from amino-ThDP to imino-ThDP is not unlikely to happen in the enzymatic environment.

Setting up similar criteria for NAC formation for all transformations in the putative tautomeric equlibrium resulted in the NAC frequencies shown in Scheme 3. The simulations clearly show that the enzyme is able to bind all three tautomers of the cofactor. On the basis of the computed

Scheme 3: Numbers of NACs Identified for the Tautomeric Conversions of ThDP

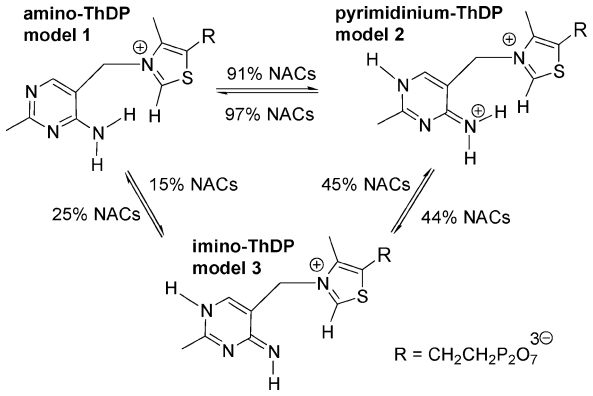

relatively high NAC numbers, it can be concluded that the cofactor binding site in the enzyme is set up to accommodate the studied tautomeric equlibrium very efficiently. Furthermore, we expect that the equilibrium between amino-ThDP and pyrimidinium-ThDP is fast, as the enzyme keeps Glu50-(OE2) and ThDP(N1′) at hydrogen-bond distance in 91% and 97% of the sampled structures, respectively. The results also indicate that imino-ThDP is likely to be formed by a two-step process with pyrimidinium-ThDP as a reactive intermediate because higher NAC frequencies are computed. Pyrimidinium-ThDP is thus an intermediate in the equilibrium between amino-ThDP and imino-ThDP, and one might therefore expect an easy conversion to both of these forms. This is in agreement with the computed high NAC frequencies for transformation of pyrimidinium-ThDP to amino-ThDP (97%) and imino-ThDP (44%). The MD simulations seem to indicate that amino-ThDP is the more stable of the two when no substrate is bound, based on the computed NAC frequencies. This is in agreement with experimental results, because the CD band indicative of the formation of imino-ThDP is only found in the presence of substrate (*14a*, *20*). It is noteworthy that the computed NAC frequencies cannot be related directly to reaction rates, because the activation energies are ignored.

Mutation Studies. We now turn our focus to the function of Glu50, which has been proposed to be the catalyst for the tautomeric equilibration. Glu50 is mutated to alanine and two water molecules (dwat1 and dwat2) in model **4**. Experimental studies report that this mutation reduces reactivity of the enzyme (*14a*, *14h*). In the course of the 2.0 ns simulation, three different water molecules are in turn located at position 3, labeled pos3, in Figure 4. Hydrogen bonding of the water molecule at pos3 to ThDP(N1′) is found throughout the simulation, with an average heteroatomic distance of 2.89 ± 0.13 Å. Most of the time, this water

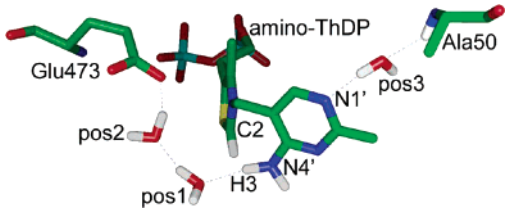

FIGURE 4: Snapshot of a NAC structure for the direct generation of imino-ThDP from amino-ThDP in mutant Glu50Ala in model **4**. Water positions are labeled pos1, pos2, and pos3. Nonpolar hydrogens are omitted for clarity.

molecule is also hydrogen-bonded to Ala50(HN) as shown in Figure 4. A NAC for formation of pyrimidinium-ThDP is defined by one distance and the corresponding angle, analogous to the wild-type case (model **1**, Figure 2), except that in the Glu50Ala mutant, the hydrogen-bonding partner is not a glutamate residue but a water molecule. The NAC criteria are fulfilled in 76% of the sampled conformations in model **4**. In the wild-type (model **1**), 91% of the sampled conformations were identified as NACs for the Glu50(HE2) to ThDP(N1′) transfer. Comparison of these NAC numbers indicates that reactive conformers are present for proton transfer to ThDP(N1′) in both simulations. A NAC for the concerted one-step formation of imino-ThDP directly from amino-ThDP in the Glu50Ala mutant is illustrated in Figure 4. Twelve percent of the sampled structures during production dynamics are identified as NACs. Again, the Glu50Ala mutant displays a NAC number that is comparable to the computed 15% NACs in the wild-type (model **1**).

On the basis of detailed studies of intramolecular reactions, it has been suggested that the more NACs formed in an E·S complex, the higher efficacy of the enzyme (*46*), and therefore, the reported NAC numbers might indicate that formation of pyrimidinium-ThDP and imino-ThDP are almost as likely in the Glu50Ala mutant as in the wild-type. However, since the otherwise powerful NAC concept does not take the activation energies and different equilibrium constants into account, further calculations are needed to address this issue quantitatively. On the basis of acidities, we assume that the activation energy for dissociation of a proton from Glu-COOH is much lower than from H_2O, also in the interior of the enzyme, and this fact is strongly favoring formation of pyrimidinium-ThDP or imino-ThDP in the wild-type (model **1**) as compared to the mutant (model **4**). We therefore believe that the reduced reactivity of the Glu50Ala mutant is a transition state effect and *not* a ground-state effect, because the simulations indicate that the binding of the cofactor is not destroyed by the Glu50Ala mutation as the cofactor binding in the Michaelis complexes of model **1** and model **4** are indeed very similar.

Glu473 is replaced by an alanine and two water molecules in active site models **5** and **6** (see Table 1). These simulations therefore address the question whether Glu473 is a unique proton acceptor in the proton relay for initial formation of imino-ThDP by deprotonation of ThDP(N4′). The intermediate in the tautomeric equilibrium, pyrimidinium-ThDP, is placed at the cofactor binding site. The conserved Asp27 is protonated and unprotonated in models **5** and **6**, respectively, to determine whether other general bases can be identified in the active site. In active site model **5**, with a protonated Asp27, several hydrogen-bonding pathways originating at ThDP(N4′) proceed through the network of water molecules. However, all are found to terminate at backbone carbonyl oxygen or amide nitrogen atoms that may function as hydrogen bond acceptors, but not as terminal proton acceptors. Therefore, no alternative proton relay pathway is identified in model **5**. For active site model **6**, with a deprotonated Asp27, a proton relay is identified from ThDP-(N4′) via a water molecule and Tyr290(OH) to Asp27(OD2) in 9.4% of the sampled structures. From these models, it is concluded that only a deprotonated Asp27 is able to function as a proton acceptor, beside Glu473. On the basis of the computed NAC frequencies, we find that Glu473 is most likely to be the primary proton acceptor for the studied deprotonation; however, Asp27 can function as such also.

Protonation States of Glu473 and Asp27. Some papers (*11*, *54*, *55*) report different protonation states of the two acidic residues Glu473 and Asp27, as compared to models **1**, **2**, and **3** discussed above. To investigate the most likely protonation states of these residues, two simulations with reversed protonation of Glu473 and Asp27 were carried out with the cofactor modeled as amino-ThDP in model **7** and as pyrimidinium-ThDP in model **8**. The proton relay from ThDP(N4′) to Glu473 is now completely blocked. In model **7**, a proton relay could be identified from ThDP(N4′) to Asp27(OD2) with the intermediacy of two water molecules, simultaneously with protonation of ThDP(N1′) by Glu50 in only 0.08% of the structures sampled during production dynamics. The NAC number for a direct generation of imino-ThDP from amino-ThDP in a wild-type apoenzyme in model **1** was 15% and thus ∼200 times more likely.

In model **8**, pyrimidinium-ThDP is placed at the cofactor binding site. Eighteen percent of the NACs are identified for a proton relay from ThDP(N4′) to the deprotonated Asp27(OD2), via only one water molecule. A second proton relay was identified from ThDP(N4′) passing through a water molecule and Tyr290(OH) terminating at Asp27(OD2) in 9.0% of the sampled conformations. Last, a third proton relay was identified from ThDP(N4′) to His114(Nϵ) with the intermediacy of one water molecule in 8.1% of the conformations. In summary, approximately 35% of NACs are identified in model **8** for a proton relay from pyrimidinium-ThDP(N4′), and out of these, 27% constitute a proton relay to Asp27(OD2). For comparison, model **2** gives 44% NACs for converting pyrimidinium-ThDP to imino-ThDP. Therefore, based on models **7** and **8**, we believe that protonated Asp27 and deprotonated Glu473 are more likely in a wild-type apoenzyme. The reversed protonation cannot be completely excluded; however, the results with a deprotonated Asp27 lead to a situation where proton flow in the active site is not controlled due to the different parallel relays, and we expect this is a less desirable situation. Overall, the simulations reveal that the relay of one of the two protons originally on ThDP(N4′) is not dependent on one residue only, Glu473; when this residue cannot function as a proton acceptor, either if it is protonated, Glu473(COOH), or mutated, Glu473Ala, other basic residues in the binding pocket can accept the proton being relayed from ThDP(N4′).

Generation of the Catalytic Active Ylide. The proposed mechanism for generation of the catalytic active ylide involves a direct intramolecular proton abstraction of ThDP-(H4) by the lone pair of imino-ThDP(N4′) (*14a*, *14h*). Searching for NAC structures for this abstraction, one distance criteria, for example, the distance between ThDP-(N4′) and ThDP(H4), must be equal to or less than 2.5 Å, and two angle criteria, linearity about the angle N4′···H4−C2 and 120° about the angle C4′−N4′···H4, must be fulfilled. For imino-ThDP (model **3**) 1.8% of NACs were identified among the sampled structures. In the initial system (*11*, *12*), a water molecule is located in hydrogen-bond distance to both ThDP(N4′) and ThDP(C2) (Figure S2 in Supporting Information). On the basis of this observation, we analyzed the 15 000 sampled conformations in model **3** for NACs for generation of the ylide, through the intermediacy of this water molecule, and 5.9% are identified as such

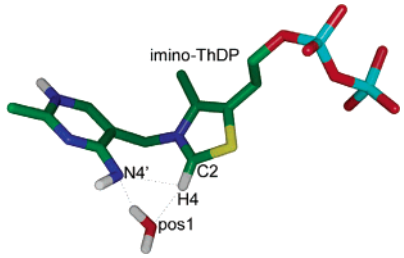

FIGURE 5: Snapshot of a NAC for generation of ylide-ThDP from imino-ThDP (model **3**) by water-mediated proton transfer. The direct transfer pathway is also marked on the figure. Nonpolar hydrogens are omitted for clarity.

(Figure 5). The NAC number for the water-mediated proton transfer for generation of the catalytic active ylide (5.9%) is thus approximately 3 times the NAC number for the direct proton transfer (1.8%), indicating that ylide generation with the intermediacy of a water molecule may be a more likely pathway. However, the direct proton transfer might have the lowest activation barrier. Calculations of the activation energies are currently in progress in our group. It is noteworthy that none of the sampled structures represent a NAC for both direct and water-mediated generation of the catalytic active ylide from the imino-ThDP structure. Friedemann et al. studied formation of the catalytic ylide by DFT methods from a N1′-deprotonated imino-type anionic ThDP species (*25a*). A similar DFT study of ylide formation from imino-ThDP is currently in progress.

Similarly, direct generation of ylide-ThDP was investigated from amino-ThDP (model **1**). A NAC for formation of the catalytic active ylide by direct intramolecular proton transfer within amino-ThDP also concerns the angle spanned by C2−H4···N4′, which must be close to linear. However, the angle, measured to be 115.8 ± 8.0° and such a large deviation from linearity for the proton transfer, is obviously the reason for the lack of NAC formation in model **1**. Ylide formation within amino-ThDP in model **1** by a water-mediated proton transfer mechanism is not likely to proceed because the water molecule is oriented with the hydrogen atoms pointing in the wrong directions throughout the simulation, as seen in Figure 2. These findings are in agreement with acidity values in water, where an exocyclic amino group has a pK_a of ∼9 (*56*), and an exocyclic ammonium ion has a pK_a of 3−5 (*57*).

It is a matter of removing pyrimidinium-ThDP(H4) to generate the catalytic important ylide directly from pyrimidinium-ThDP. With regard to heteroatomic distances, a proton relay pathway is present from ThDP(H4) to Glu473-(OE2) with the intermediate of two water molecules in 27% of the time in model **2**. However, taking protons into account, this pathway is completely inhibited, because the first water molecule in that relay is oriented incorrectly for hydrogen bonding to ThDP(H4). The simulations indicate that no other general base lining the substrate binding pocket (Asp27, His113, and His114) is able to activate the thiazolium ring directly, as no such proton-transfer pathways can be identified from the MD trajectories. Washabaugh et al. suggested a base in the active site as being responsible for a direct deprotonation of the thiazolium ring, forming the catalytic active ylide-ThDP (*15*), but this could not be found in any of our simulations.

Substrate Binding. To understand in detail the mechanism of the reaction catalyzed by PDC, it is of vital importance to learn how the substrate binds in the active site. This is a difficult task to address experimentally; however, MD simulations can be very helpful for getting further information about substrate binding. The papers by Lobell and Crout (*23*) and by Tittmann et al. (*58*) include figures proposing binding modes of pyruvate in the active site. These substrate bindings are based on indirect evidence, as they, for example, are deduced from observed changes in the distribution of *isolated* products and covalently bonded ThDP intermediates of mutated enzymes as measured by NMR in the absence of the enzyme (*58a*). The variation in distribution of products and intermediates led the investigators, in a very elegant way, to deduce at what stage of the reaction the various mutated amino acid residues play important roles (*58a*). From this observation, the mode of interaction between the enzyme and the reacting species was constructued. For example, Glu473 was found to be important for the C−C bond formation; thus, it was logically concluded that Glu473 must interact with the substrate in the Michaelis complex. Exactly how this interaction takes place cannot be extracted from this type of experiment.

In Figure 6, the average structure for the binding of pyruvate in the active site is displayed based on the trajectory from model **9**. The identified hydrogen bonds between substrate and active site amino acid residues are indicated. The simulation reveals that pyruvate is placed under the thiazolium ring of ThDP. The substrate is oriented such that the pyruvate carboxyl group resides near the positively charged ylide-ThDP(N3) (3.81 ± 0.19 Å) and the methyl group near ylide-ThDP(S) (3.93 ± 0.33 Å). Three conserved hydrogen bonds between pyruvate and active site residues are identified. The carboxylate group of pyruvate forms one hydrogen bond to Glu473(OE2) with a distance of 2.59 ± 0.08 Å and an angle around the hydrogen of 163.7 ± 8.2°. Another hydrogen bond to Asp27(HN) with a distance of 2.81 ± 0.13 Å and an angle measuring 154.9 ± 8.7° is identified. The third hydrogen bond is found between the carbonyl oxygen of the substrate and Tyr290(OH) with an average distance of 2.74 ± 0.16 Å and an angle of 148 ± 11°. Tittmann et al. suggested, based on their NMR experiments of isolated products and covalent-ThDP intermediates (*58a*), that pyruvate could form hydrogen bonds to Glu473 and ThDP(N4′); the latter should then transfer a proton upon the nucleophilic attack to the substrate. The hydrogen bond proposed by Tittmann et al. between Glu473 and the carboxylate group of the substrate is indeed conserved throughout the MD simulation. Even though we started the simulation with a docked pyruvate substrate in a position where it is able to form a hydrogen bond to ThDP(N4′), the substrate immediately rotated slightly away from this position during equilibration, thereby inhibiting a direct interaction between pyruvate(O1) and ylide-ThDP(N4′). We are not able to identify a hydrogen bond between the substrate and ylide-ThDP(N4′) at any time throughout production dynamics. The distance from pyruvate(O1) to ylide-ThDP(N4′) was measured to 3.81 ± 0.33 Å, which, even in the lower limit, is not a hydrogen bond, and the angle was far from linear. The binding of pyruvate, as revealed from this MD simulation, is very similar to the experimentally reported binding of the substrate analogue, pyruvamide, in YPPC where the shortest possible hydrogen bond distance between ThDP(N4′) and pyruvamide is 3.85 Å (*13*e). From inspection of the average

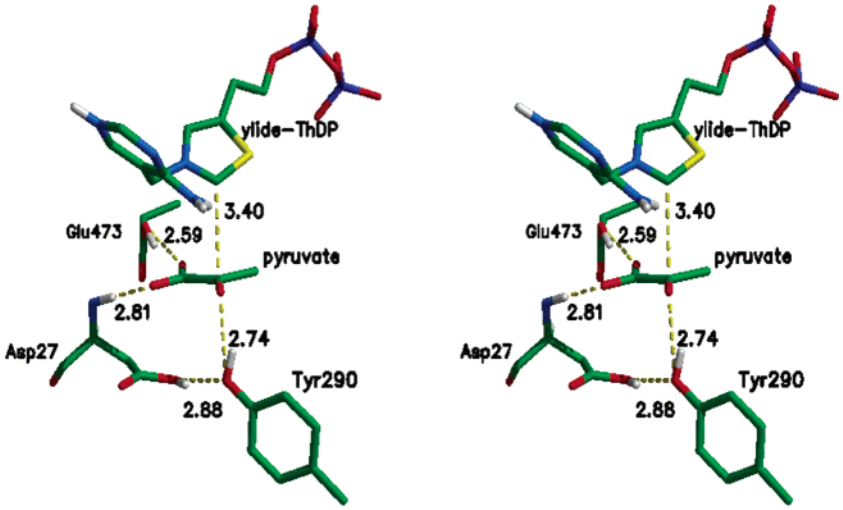

FIGURE 6: Stereoplot of the average structure for binding of pyruvate in the active site calculated from model **9**. Important hydrogen bonds between substrate and active site residues are shown along with the nucleophilic attacking distance from ylide-ThDP(C2) to pyruvate(C2). All distances are heteroatomic distances and are displayed in angstroms (Å). Important polar hydrogen atoms are included for clarity.

structure of the Michaelis complex, it is plausible that the hydrogen bond between ThDP(N4′) and pyruvate(O2) cannot form at this stage of the reaction. To carry out the nucleophilic attack, the geometric orientation of the 2-oxo functionality of the substrate is not pointing toward ThDP-(N4′). However, the structure in Figure 6 does not rule out that this hydrogen bond may be found in the tetrahedral intermediate, lactyl-ThDP. The re-hybridization of pyruvate-(C2) from sp^2 to sp^3 on formation of lactyl-ThDP will push the oxygen atom in question further away from ThDP, whereas the decrease in separation between ThDP and pyruvate upon bond formation will work in the opposite direction. Further calculations on lactyl-ThDP are thus needed to address this possibility quantitatively.

Nucleophilic Attack. Expecting that the nucleophilic lone-pair of ylide-ThDP(C2) lies in the plane of the thiazolium ring, we have to make sure that pyruvate(C2) is also placed close to this plane. An indication of correct positioning of the reacting groups can be found by measuring the dihedral angle ThDP(C_{br})−ThDP(N3)−ThDP(C2)···pyruvate(C2). To be properly oriented, this dihedral angle must be *syn*. A dihedral of 52.0 ± 8.9° is measured, showing that the two reacting substrates are in a good intermolecular arrangement. The nucleophilic attacking distance, ylide-ThDP(C2)··· pyruvate(C2), and angle, ylide-ThDP(C2)···pyruvate(C2)− pyruvate(O1), are plotted in Figure 7. It can be seen that the separation and orientation of the two reacting molecules are fine; 41% of all sampled structures during reaction dynamics possess a separation between the nucleophile and the carbonyl carbon atom of less than 3.4 Å and an attacking angle within 15° of the Bürgi−Dunitz angle of 107° (*59*). Ylide-ThDP is thus positioned correctly for a nucleophilic attack at the carbonyl group from the *si*-side of the substrate leading to formation of *S*-lactyl-ThDP, in agreement with previous proposals (*23*, *55*). The simulation also allows for studies of other potentially stabilizing interactions to the evolving intermediate apart from the hydrogen bond between pyruvate(O1) and ThDP(N4′).

On the basis of our findings, we want to propose an alternative way for stabilization of the evolving negative charge when the nucleophilic ylide-ThDP(C2) attacks the substrate, namely, via the protons on Tyr290(OH) and

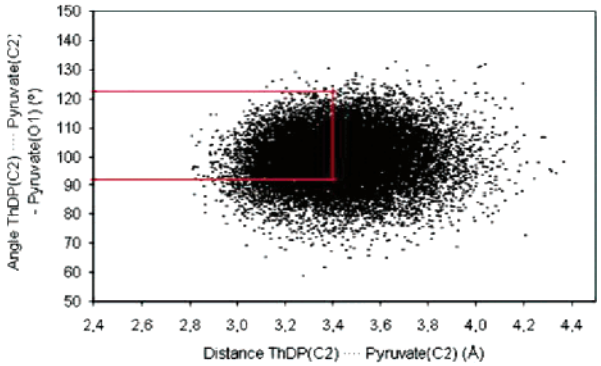

FIGURE 7: The nucleophilic attacking distance, ylide-ThDP-(C2)···pyruvate(C2), is plotted against the attack angle, ylide-ThDP-(C2)···pyruvate(C2)−pyruvate(O1). Area with NACs is enclosed by red lines.

Asp27(OD2). The proposed reaction mechanism is displayed in Scheme 4. The heteroatomic distance between the two oxygen atoms in question is measured to be 2.88 ± 0.31 Å with the corresponding hydrogen bond angle spanned by Tyr290(OH)···Asp27(HD2)−Asp27(OD2) measuring 146 ± 24°. If this proposed proton relay is functioning in the active enzyme, the MD simulation must reveal this in the computed NAC frequency for such an attack. Upon inclusion of the two hydrogen bonds for a full proton relay, NACs are present in 12.7% of all structures for this nucleophilic attack. The consequence of the hypothesized mechanism for stabilization of the evolving negative charge is that Asp27 becomes deprotonated as the lactyl-ThDP intermediate forms (see Scheme 1). This is in fine agreement with Jordan's experimental findings from kinetic observations of k_{cat} and k_{cat}/K_M stating that Asp27 remains protonated until formation of lactyl-ThDP (*14a*). Some reports suggest that Asp27 becomes deprotonated after decarboxylation by transferring the proton to the anionic/enamine-ThDP intermediate (*58a*). According to a very recent study by Tittmann et al., the exact place along the reaction coordinate for deprotonation of Asp27 remains unclear (*58b*). Our simulations can accommodate both possibilities, as His113 is placed in hydrogen-bonding distance to Asp27 throughout the simulation (data not shown), and it is therefore possible to transfer a proton from His113

Scheme 4: Proposed Reaction Mechanism for the Nucleophilic Attack of Ylide-ThDP on Pyruvate

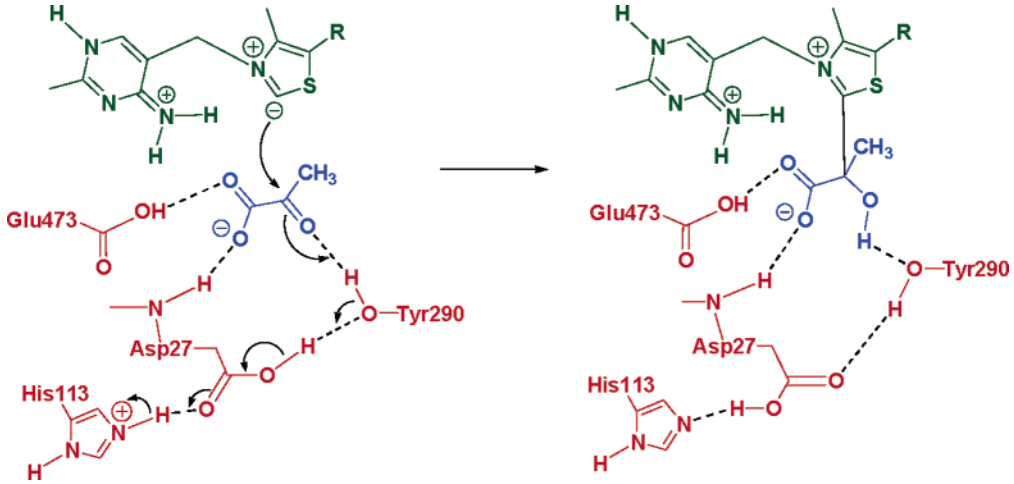

to Asp27 upon the nucleophilic attack. This possibility is included in Scheme 4.

CONCLUSIONS AND PERSPECTIVES

Several proton transfer processes related to the activation of ThDP in ZmPDC as well as substrate binding are presented. We have used MD simulations to study the dynamics and stability of the different tautomers in ThDP-dependent reactions. The simulations show that the three tautomers of ThDP all bind at the cofactor binding site by forming very similar interactions with the amino acid residues lining the binding pocket. The possible involvement of a tautomeric equilibrium between amino-ThDP and imino-ThDP was found likely because high frequencies for formation of NACs were identified. The computed NAC frequencies indicate that pyrimidinium-ThDP is a reactive intermediate in the equilibrium. Therefore, the simulations support the proposal of the tautomeric equilibrium as being a two-step reaction. All simulated models that include the wild-type holoenzyme identified a proton relay pathway from ThDP-(N4′) to the conserved residue Glu473 with the intermediacy of two water molecules, indicating that a primary role of Glu473 may be to act as a general base in the formation of imino-ThDP. This finding is a slight modification of the proposal by Jordan that in YPDC the primary function of Glu473 may be to deprotonate N4′ with the intermediacy of only one water molecule (*14a*). Computed NAC frequencies indicate that the tautomeric equilibrium may be shifted in favor of the amino-ThDP, in agreement with CD experiments in the absence of substrate (*20*), but also that the enzyme provides a very dynamic environment to support the tautomeric equilibrium of the cofactor.

The mutant Glu50Ala enzyme with bound amino-ThDP displays NAC numbers for generation of pyrimidinium-ThDP, as well as for direct generation of imino-ThDP, that are comparable to those obtained from the models with the wild-type holoenzyme. As activation energies are ignored in the present study, the simulations do *not* conclude that the rates of the transitions are comparable in the mutant and wild-type apoenzymes. However, based on the similar NAC frequencies in the wild-type and Glu50Ala mutated enzymes, we conclude that the experimentally observed decrease in catalytic proficiency must be a transition state effect because the two Michaelis complexes studied for the apoenzyme and the Glu50Ala mutated enzyme show very similar binding with no indications of ground-state destabilization of the Michaelis complex (*60*).

The most likely protonation states of the conserved residues Asp27 and Glu473 until formation of imino-ThDP are proposed to be protonated and deprotonated, respectively. The mutant Glu473Ala enzyme with bound pyrimidinium-ThDP showed no alternative proton relay pathway for generation of imino-ThDP when Asp27 is protonated. Changing the protonation state of Asp27 to unprotonated for the Glu473Ala mutant showed a possible proton relay from ThDP(N4′) to Asp27, implying that when "knocking out" the primary proton acceptor, Glu473, the conserved residue Asp27 is able to function as a proton acceptor. Experimentally, it is known that Glu473Asp mutated ZmPDC is almost unaffected with respect to ylide formation (*58*). Within our model, this can be explained if Asp27 takes over the role in imino-ThDP generation. It would be very interesting to test this hypothesis experimentally by studying the kinetic effects of a double mutation, Asp27Ala and Glu473Ala.

On the basis of NAC numbers, we propose that generation of the ylide can proceed either direct or via one water molecule. The latter pathway represents a minor revision of the mechanism for ylide generation that has so far been suggested to proceed by a direct intramolecular proton transfer from C2 by the N4′ nitrogen lone pair (*12*). Further calculations of activation energies are needed to fully account for the reaction pathway for the proton transfer forming ylide-ThDP. We found that generation of ylide-ThDP is only possible from imino-ThDP. No proton relay pathway could be identified directly from the C2-carbon atom to a general base in the active site. In that way, the data presented in this work provide a model for the activation of ThDP in ZmPDC that is consistent with the proposals of Jordan et al. (*14h*), Kern et al. (*14i*), and others (*14*) stating that the two nitrogen atoms, N1′ and N4′, of the aminopyrimidine ring contribute significantly to the activation. Also, the simulations explain why the otherwise less important imino-ThDP plays a significant role in the reaction, as only this tautomer can be activated to form the catalytically important nucleophilic ylide-ThDP. To further investigate the proton-transfer processes in the activation of ThDP, a QM/MM model will be constructed (*61*). This setup can answer the question whether the transfer occurs as a fast concerted or a stepwise event

(*53*) and can take into account the activation barriers. Work along these lines is in progress.

Finally, we examined the binding of the substrate. Even though we initially docked pyruvate to form a hydrogen bond from pyruvate(O1) to ThDP(N4′), the simulation revealed that this indeed is not a preferred binding orientation in the Michaelis complex. During the initial equilibration, the substrate rotated to form a hydrogen bond between pyruvate-(O1) and Tyr290(OH). We may speculate that this otherwise attractive interaction between pyruvate(O1) and ThDP(N4′) is not compatible with the geometric requirements for the nucleophilic attack of ylide-ThDP(C2) on the substrate. From the simulations, we cannot rule out that a concerted nucleophilic attack and substrate rotation take place leading to the formation of this hydrogen bond as the covalent bond between ThDP(C2) and pyruvate(C2) forms. The carbonyl carbon atom of the substrate will re-hybridize upon the nucleophilic attack, from sp^2 to sp^3, which will make the forming hydroxyl group point away from the plane of the thiazole ring. Further calculations on the lactyl-ThDP intermediate are needed to fully judge on this aspect quantitatively. At later stages during the catalytic cycle, like the enamine-ThDP, where an X-ray structure for yeast transketolase exists, a weak hydrogen bond has been proposed between ThDP(N4′) and the hydroxyl group (*62*). At this reaction step, the hybridization of the substrate α-carbon atom has once again changed, which gives rise to a reorientation of the adduct. Our finding that this specific hydrogen bond is not present in the Michaelis complex does not rule out that it can form at a later reaction step. In a recent crystallographic study of branched-chain 2-oxo acid dehydrogenase (E1) with a bound substrate analogue, missing the 2-oxo functionality, it was similarly suggested that, in the Michealis complex, the substrate carbonyl oxygen atom does not interact with ThDP(N4′) (*63*).

From the simulations, a different proton relay upon nucleophilic attack can be proposed for ZmPDC. We propose that simultaneously with the nucleophilic attack of the ylide-ThDP(C2) at the substrate, Asp27 transfers its proton to Tyr290(OH) which then protonates the substrate hereby forming lactyl-ThDP; see Scheme 4. At the same time, His113 is placed within hydrogen-bonding distance to Asp27 throughout the simulation and can also be involved in the outlined proton relay. However, this proton relay most likely is limited to ZmPDC, as Tyr290 is not a conserved residue. In the recent structural study on a similar dehydrogenase, it was proposed that the proton transferred to the substrate upon nucleophilic attack originated from a histidine residue, as in our model, however, passing through a water molecule (*63*).

Involvement of tyrosine residues in proton relays, even at a low pH of 6, has been studied for other enzymes such as, for example, class C β-lactamase. For this enzyme, a similar mechanism was proposed that involves a proton shuttle including a tyrosine. Like in our tentative mechanism for ZmPDC, this tyrosine immediately accepts another proton, in the case of the β-lactamase, from a neighboring Lys residue (*64*). It would be very interesting to measure the catalytic consequences of a Tyr290Phe mutation of ZmPDC: from our simulations, an effect can be expected. The catalytic cycle can proceed, as displayed in Scheme 1, with the possibility of the general acid in the conversion of the enamine-ThDP to the hydroxyethyl-ThDP being Glu473, Asp27, or, as proposed by Friedemann et al., the N4′-amino group of the pyrimidine ring (*25a*). The reprotonation of Asp27 may be possible to carry out via His113 or via the recently proposed "slinky cycle" where the two active sites in the tight dimer of ThDP-dependent enzymes display ping-pong catalysis with a proton moving back and forth between the two active sites along the catalytic cycle (*65*). Further analyses are needed to elucidate these latter proposals.

ACKNOWLEDGMENT

Computations were made possible through allocations of computer time at the SGI Origin 2000 at Aarhus University under the Danish Center for Scientific Computing.

SUPPORTING INFORMATION AVAILABLE

A list with the assignments of the protonation states of histidine residues is provided (S1). Also included are residue topology descriptions and added force constants to model the three different ThDP tautomers, ylide-ThDP, citrate, and the substrate, pyruvate. Cofactor overlay (S2) is included along with the SBMD-setup (S3). Figures illustrating the rmsd of C_α-atoms (S4−S8), positional fluctuations of the C_α-atoms in the reaction region (S9−S13), and (Φ_P,Φ_T)-plots for the cofactors (S14) are also provided. Complete citations for refs *31a* and *35* are listed. This material is available free of charge via the Internet at http://pubs.acs.org.

REFERENCES

1. Berg, J. M., Tymoczko, J. L., and Stryer, L. (2002) Glycolysis, in *Biochemistry*, 5th ed., pp 428−443, W. H. Freeman and Company, New York.
2. Williams, R. R., and Spies, T. D. (1938) *Vitamin B1 and Its Use in Medicine*, Macmillan, New York.
3. Kluger, R. (1987) Thiamin diphosphate: a mechanistic update on enzymic and nonenzymic catalysis of decarboxylation, *Chem. Rev. 87*, 863−876.
4. Mizuhara, S., and Handler, P. (1954) Mechanism of thiamine-catalyzed reactions, *J. Am. Chem. Soc. 76*, 571−573.
5. Breslow, R. (1958) On the mechanism of thiamine action. IV.[1] Evidence from studies on model systems, *J. Am. Chem. Soc. 80*, 3719−3726.
6. Schowen, R. L. (1998) Thiamin-dependent enzymes, in *Comprehensive Biological Catalysis—A Mechanistic Reference* (Sinnott, M., Ed.) Vol. II, pp 217−266, Academic Press, London, U.K.
7. Karimian, K., Mohtarami, F., and Askari, M. (1981) Mechanism of base-catalyzed Hydrogen−Deuterium exchange in thiazolium ion: Evidence for the involvement of a tetrahedral intermediate, *J. Chem. Soc., Perkin Trans 2*, 1538−1543.
8. Schörken, U., and Sprenger, G. A. (1998) Thiamin-dependent enzymes as catalysts in chemoenzymatic syntheses, *Biochim. Biophys. Acta 1385*, 229−243.
9. Pohl, M., Lingen, B., and Müller, M. (2002) Thiamin-diphosphate-dependent enzymes: New aspects of asymmetric C−C bond formation, *Chem.—Eur. J. 8*, 5289−5295.
10. Miyazaki, M., Shibue, M., Ogino, K., Nakamura, H., and Maeda, H. (2001) Enzymatic synthesis of pyruvic acid from acetaldehyde and carbon dioxide, *Chem. Commun. 18*, 1800−1801.
11. Dobritzsch, D., König, S., Schneider, G., and Lu, G. (1998) High-resolution crystal structure of pyruvate decarboxylase from *Zymomonas mobilis*. Implications for substrate activation in pyruvate decarboxylase, *J. Biol. Chem. 273*, 20196−20204.
12. Arjunan, P, Umland, T., Dyda, F., Swaminathan, S., Furey, W., Sax, M., Farrenkopf, B., Gao, Y., Zhang, D., and Jordan, F. (1996) Crystal structure of the thiamin diphosphate-dependent enzyme pyruvate decarboxylase from the yeast *Saccharomyces cerevisiae* at 2.3 Å resolution, *J. Mol. Biol. 256*, 590−600.
13. (a) Dyda, F., Furey, W., Swaminathan, S., Sax, M., Farrenkopf, B., and Jordan, F. (1993) Catalytic centers in the thiamin diphosphate dependent enzyme pyruvate decarboxylase at 2.4-Å resolution, *Biochemistry 32*, 6165−6170, (b) Lindqvist, Y.,

Schneider, G., Ermler, U., and Sundstrom, M. (1992) Three-dimensional structure of transketolase, a thiamine dependent enzyme, at 2.5 Å resolution, *EMBO J. 11*, 2373−2379, (c) Muller, Y. A., and Schulz, G. E. (1993) Structure of the thiamine- and flavin-dependent enzyme pyruvate oxidase, *Science 259*, 965−967, (d) Muller, Y. A., Schumacher, G., Rudolph, R., and Schulz, G. E. (1994) The refined structures of a stabilized mutant and of wild-type pyruvate oxidase from *Lactobacillus plantarum*, *J. Mol. Biol. 237*, 315−335, (e) Lu, G., Dobritzsch, D., Baumann, S., Schneider, G., and König, S. (2000) The structural basis of substrate activation in yeast pyruvate decarboxylase, *Eur. J. Biochem. 267*, 861−868.

14. (a) Jordan, F. (2003) Current mechanistic understanding of thiamin diphosphate-dependent enzymatic reactions, *Nat. Prod. Rep. 20*, 184−201, (b) Jordan, F., and Marian, Y. H. (1978) N1′-Methylthiaminium diiodide. Model study on the effect of a coenzyme bound positive charge on reaction mechanisms requiring thiamin pyrophosphate, *J. Am. Chem. Soc. 100*, 2534−2541, (c) Jordan, F., Chen, G., Nishikawa, S., and Sundoro-Wu, B. (1982) Potential roles of the aminopyrimidine ring in thiamin catalyzed reactions, *Ann. N.Y. Acad. Sci. 378*, 14−31, (d) Jordan, F. (1982) Role of the aminopyridine ring in thiamin-catalyzed reactions. II. Proton NMR evidence for high barriers to amino group rotation in 4-aminopyrimidines, including thiamin, at low pH in water, *J. Org. Chem. 47*, 2748−2753, (e) Schellenberger, A. (1982) The amino group and steric factors in thiamin catalysis, *Ann. N.Y. Acad. Sci. 378*, 51−62, (f) Schellenberger, A. (1990) Die Funktion der 4′-Aminopyrimidin-Komponente im Katalysemechanismus von Thiaminpyrophosphat-Enzymen aus heutiger Sicht, *Chem. Ber. 123*, 1489−1494, (g) Golbik, R., Neef, H., Hübner, G., König, S., Seliger, B., Meshalkina, L., Kochetov, G. A., and Schellenberger, A. (1991) Function of the aminopyrimidine part in thiamine pyrophosphate enzymes, *Bioorg. Chem. 19*, 10−17, (h) Kern, D., Kern, G., Neef, H., Tittmann, K., Killenberg-Jabs, M., Wikner, C., Schneider, G., and Hübner, G. (1997) How thiamine diphosphate is activated in enzymes, *Science 275*, 67−70, (i) Hübner, G., Tittmann, K., Killenberg-Jabs, M., Schäffner, J., Spinka, M., Neef, H., Kern, D., Kern, G., Schneider, G., Wikner, C., and Chisla, S. (1998) Activation of thiamin diphosphate in enzymes, *Biochim. Biophys. Acta 1385*, 221−228.

15. (a) Crane, E. J., Vaccaro, J. A., and Washabaugh, M. W. (1993) Single-turnover studies of brewer's yeast pyruvate decarboxylase: C(2)-proton transfer from thiamin diphosphate, *J. Am. Chem. Soc. 115*, 8912−8917, (b) Harris, T. K., and Washabaugh, M. W. (1995) Distribution of the thiamin diphosphate C(2)-proton during catalysis of acetaldehyde formation by brewers' yeast pyruvate decarboxylase, *Biochemistry 34*, 13994−14000.

16. (a) Katritzky, A. R., and Karelson, M. (1991) AM1 calculations of reaction field effects on the tautomeric equilibria of nucleic acid pyrimidine and purine bases and their 1-methyl analogs, *J. Am. Chem. Soc. 113*, 1561−1566, (b) Kiruba, G. S. M., and Wong, M. W. (2003) Tautomeric equilibria of pyridoxal-5′-phosphate (Vitamin B_6) and 3-hydroxypyridine derivatives: A theoretical study of solvation effects, *J. Org. Chem. 68*, 2874−2881, (c) Neely, R. K., Magennis, S. W., Dryden, D. T. F., and Jones, A. C. (2004) Evidence of tautomerism in 2-aminopurine from fluorescence lifetime measurements, *J. Phys. Chem. B 108*, 17606−17610, (d) Headley, A. D., and Starnes, S. D. (1995) Effects of branching on the tautomeric equilibrium of amino acids, *J. Am. Chem. Soc. 117*, 9309−9313, (e) Lanyi, J. K. (1997) Mechanism of ion transport across membranes. Bacteriorhodopsin as a prototype for a proton pumps, *J. Biol. Chem. 272*, 31209−31212, (f) Morgan, A. R. (1993) Base mismatches and mutagenesis: how important is tautomerism?, *Trends Biochem. Sci. 18*, 160−163, (g) Mitchell, P. (1961) Coupling of phosphorylation to electron and hydrogen transfer, *Nature 191*, 144−148, (h) Freedman, H., Nguyen H. N., and Troung, T. N. (2004) A study of the tautomeric equilibria of 2-hydroxypyridine/2-oxopyridine and of cytosine in water using the coupled reference interaction site model(RISM)/molecular dynamics (MD) approach, *J. Phys. Chem. B 108*, 19043−19048.

17. Metzler, D. E., Harris, C. M., Johnson, R. J., Siano, D. B., and Thomson, J. A. (1973) Purification and characterization from *Chromobacterium violaceum* of an enzyme catalyzing the synthesis of γ-cyano-α-aminobutyric acid and thiocyanate, *Biochemistry 12*, 5377−5392.

18. (a) Vaz, E., Muñoz, L., and Llor, J. (2004) Study of the tautomeric equilibrium of pyridoxine in 1,4-dioxane/water mixtures by ^{13}C nuclear magnetic resonance. Thermodynamic characterization and solvent effects, *J. Org. Chem. 69*, 6387−6393, (b) Llor, J., and Muñoz, L. (2000) Tautomeric equilibrium of pyridoxine in water. Thermodynamic characterization by ^{13}C and ^{15}N nuclear magnetic resonance, *J. Org. Chem. 65*, 2716−2722, (c) Llor, J., Lopez-Mayorga, O., and Muñoz, L. (1993) Thermodynamic characterization of tautomeric equilibria by multinuclear magnetic resonance. Application to 3-hydroxypyridine, *Magn. Reson. Chem. 31*, 552−556.

19. (a) Eventova, I., Nadler, E. B., Rochlin, E., Frey, J., and Rappoport, Z. (1993) Stable simple enols. 33. Effect of tetra-*m*-bromo and tetra-*m*-methyl buttressing on the ground-state structures, rotational barriers, and keto ⇌ enol equilibria of 2,2-dimesityl-1-R-ethenols, *J. Am. Chem. Soc. 115*, 1290−1302, (b) Mukhopadhyaya, J. K., Sklenak, S., and Rappoport, Z. (2000) Cyano-, nitro-, and alkoxycarbonyl-activated observable stable enols of carboxylic acid amides, *J. Org. Chem. 65*, 6856−6867, (c) Lei, Y. X., Cerioni, G., and Rappoport, Z. (2001) Enols of amides. The effect of fluorine substituents in the ester groups of dicarboalkoxyanilidomethanes on the enol/amide and *E*-enol/Z-enol ratios. A multinuclei NMR study, *J. Org. Chem. 66*, 8379−8394, (d) Kim, J. Y., Kim, G., Kim, C. R., Lee, S. H., Lee, J. H., and Kim, J. S. (2003) UV band splitting of chromogenic azo-coupled calix[4]-crown upon cation complexation, *J. Org. Chem. 68*, 1933−1937, (e) Godsi, O., Turner, B., Suwinska, K., Peskin, U., and Eichen, Y. (2004) Enol-enamine tautomerism in crystals of 1,3-bis(pyridin-2-yl) propan-2-one: A combined crystallographic and quantum-chemical investigation of the effect of packing on tautomerization processes *J. Am. Chem. Soc. 126*, 13519−13525.

20. (a) Jordan, F., Zhang, Z., and Sergienko, E. (2002) Spectroscopic evidence for participation of the 1′,4′-imino tautomer of thiamin diphosphate in catalysis by yeast pyruvate decarboxylase, *Bioorg. Chem. 30*, 188−198, (b) Jordan, F., Nemeria, N. S., Zhang, S., Yan, Y., Arjunan, P., and Furey, W. (2003) Dual catalytic apparatus of the thiamin diphosphate coenzyme: Acid−base via the 1′,4′-iminopyrimidine tautomer along with its electrophilic role, *J. Am. Chem. Soc. 125*, 12732−12738, (c) Nemeria, N., Baykal, A., Joseph, E., Zhang, S., Yan, Y., Furey, W., and Jordan, F. (2004) Tetrahedral intermediates in thiamin diphosphate-dependent decarboxylations exist as a 1′,4′-imino tautomeric form of the coenzyme, unlike the Michaelis complex or the free coenzyme, *Biochemistry 43*, 6565−6575.

21. Jordan, F., Baburina, I., Gao, Y., Kahyaoglu, A., Nemeria, N., Volkov, A., Yi, J.-Z., Zhang, D., Machado, R., Guest, J. R., Furey, W., and Hohmann, S. (1996) New insights to the regulation of thiamin diphosphate dependent decarboxylases by substrate and ThDP. Mg(II), in *Biochemistry and Physiology of Thiamin Diphosphate Enzymes*, (Bisswanger, H. and Schellenberger, A., Eds.) pp 53−69, A. u. C. Intemann Verlag, Prien, Germany.

22. Schenk, G., Leeper, F. J., England, R., Nixon, P. F., and Duggleby, R. G. (1997) The role of His113 and His114 in pyruvate decarboxylase from *Zymomonas mobilis*, *Eur. J. Biochem. 248*, 63−71.

23. Lobell, M., and Crout, D. H. G. (1996) Pyruvate decarboxylase: A molecular modeling study of pyruvate decarboxylation and acyloin formation, *J. Am. Chem. Soc. 118*, 1867−1873.

24. (a) von Fircks, A., Naumann, S., Friedemann, R., and König, S. (1996) Molecular dynamics simulations on the coenzyme thiamin diphosphate in apoenzyme environment, *J. Mol. Model. 2*, 312−318, (b) Friedemann, R., von Fircks, A., and Naumann, S. (1998) GROMOS-MD simulations on the coenzyme thiamin diphosphate in apoenzyme environment, *Int. J. Quantum Chem. 70*, 407−413.

25. (a) Friedemann, R., Tittmann, K., Golbik, R., and Hübner, G (2004) DFT studies on key intermediates in thiamin catalysis, *Int. J. Quantum Chem. 99*, 109−114, (b) Friedemann, R., and Naumann, S. (2003) Ab initio and DFT calculations on the initial step in thiamin catalysis, *J. Mol. Struct. (THEOCHEM) 630*, 275−281, (c) Friedemann, R., Neef, H. (1998) Theoretical studies on the electronic and energetic properties of the aminopyrimidine part of thiamin diphosphate, *Biochim. Biophys. Acta 1385*, 245−250, (d) Friedemann, R., and Breitkopf, C. (1996) Theoretical studies on the decarboxylation reaction in thiamin catalysis, *Int. J. Quantum Chem. 57*, 943−948.

26. (a) Luo, J., and Bruice, T. C. (2001) Dynamic structures of horse liver alcohol dehydrogenase (HLADH): Results of molecular dynamics simulations of HLADH-NAD^+-$PhCH_2OH$, HLADH-NAD^+-$PhCH_2O^-$, and HLADH-NADH-PhCHO, *J. Am. Chem. Soc. 123*, 11952−11959, (b) Valiña, A. L. B., Mazumder-Shivakumar, D., and Bruice, T. C. (2004) Probing the Ser-Ser-Lys catalytic triad mechanism of peptide amidase: Computational

studies of the ground state, transition state, and intermediate, *Biochemistry 43*, 15657−15672, (c) Schiøtt, B., and Bruice, T. C. (2002) Reaction mechanism of soluble epoxide hydrolase: Insights from molecular dynamics simulations, *J. Am. Chem. Soc. 124*, 14558−14570.
27. Chang, A. K., Nixon, P. F., and Duggleby, R. G. (1999) Aspartate-27 and glutamate-473 are involved in catalysis by *Zymomonas mobilis* pyruvate decarboxylase, *Biochem. J. 339*, 255−260.
28. König, S. (1998) Subunit structure, function and organisation of pyruvate decarboxylases from various organisms, *Biochim. Biophys. Acta 1385*, 271−286.
29. Brooks, C. L., III, and Karplus, M. (1989) Solvent effects on protein motion and protein effects on solvent motion: Dynamics of the active site region of lysozyme, *J. Mol. Biol. 208*, 159−181.
30. Brooks, B. R., Bruccoleri, R. E., Olafson, B. D., States, D. J., Swaminathan, S., and Karplus, M. (1983) CHARMM: A program for macromolecular energy, minimization, and dynamics calculations, *J. Comput. Chem. 4*, 187−217.
31. (a) MacKerell, A. D., Jr., et al. (1998) All-atom empirical potential for molecular modeling and dynamics studies of proteins, *J. Phys. Chem. B 102*, 3586−3616, (b) Pavelites, J. J., Gao, J., Bash, P. A., and Mackerell, A. D. M., Jr. (1997) A molecular mechanics force field for NAD^+ NADH, and the pyrophosphate groups of nucleotides *J. Comput. Chem. 18*, 221−239.
32. (a) Foloppe, N., and MacKerell, A. D., Jr. (2000) All-atom empirical force-field for nucleic acids. 1) Parameter optimization based on small molecule and condensed phase macromolecular target data, *J. Comput. Chem. 21*, 86−104, (b) MacKerell, A. D., Jr., and Banavali, N. (2000) All-atom empirical force-field for nucleic acids. 2) Application to molecular simulations of DNA and RNA in solution, *J. Comput. Chem. 21*, 105−120.
33. Berman, H. M., Westbrook, J., Feng, Z., Gilliland, G., Bhat, T. N., Weissig, H., Shindyalov, I. N., and Bourne, P. E. (2000) The protein data bank, *Nucleic Acids Res. 28*, 235−242.
34. (a) MidasPlus Version 2.1, Computer Graphics Lab., University of California, San Francisco, CA (1997), (b) Ferrin, T. E., Huang, C. C., Jarvis, L. E., and Langridge, R. (1988) The MIDAS display system, *J. Mol. Graphics 6*, 13−27.
35. Frisch, M. J., et al. (1998) *Gaussian 98*, revision A.7, Gaussian, Inc., Pittsburgh, PA.
36. Besler, B. H., Merz, K. M., and Kollman, P. A. (1990) Atomic charges derived from semiempirical methods, *J. Comput. Chem. 11*, 431−439.
37. Sigfridsson, E., and Ryde, U. (1998) Comparison of methods for deriving atomic charges from the electrostatic potential and moment, *J. Comput. Chem. 19*, 377−395.
38. Bayly, C. I., Cieplak, P., Cornell, W. D., and Kollman, P. A. (1993) A well-behaved electrostatic potential based method using charge restraints for deriving atomic charges: the RESP model, *J. Phys. Chem. 97*, 10269−10280.
39. Accelrys (2000), Quanta 2000, San Diego, CA.
40. Jorgensen, W. L., Chandrasekhar, J., Madura, J. D., Impley, R. W., and Klein, M.-L. (1983) Comparison of simple potential functions for simulating liquid water, *J. Chem. Phys. 79*, 925−935.
41. Verlet, L. (1967) Computer "experiments" on classical fluids. I. Thermodynamical properties of Lennard-Jones molecules, *Phys. Rev. 159*, 98−113.
42. Leach, A. R. (2002) *Molecular Modelling: Principles and Applications*, 2nd ed., Prentice Hall, New York.
43. McCammon, J. A., and Harvey, S. C. (1987) *Dynamics of Proteins and Nucleic Acids*, Cambridge University Press, Cambridge, U.K.
44. Steinbach, P. J., and Brooks, B. R. (1994) New spherical-cutoff methods for long-range forces in macromolecular simulation, *J. Comput. Chem. 15*, 667−683.
45. Ryckaert, J. P., Ciccotti, G., and Berendsen, H. J. C. (1977) Numerical integration of the Cartesian equations of motion of a system with constraints: molecular dynamics of *n*-alkanes, *J. Comput. Phys. 23*, 327−341.
46. (a) Lightstone, F. C., and Bruice, T. C. (1996) Ground state conformations and entropic and enthalpic factors in the efficiency of intramolecular and enzymatic reactions. 1. Cyclic anhydride formation by substituted glutarates, succinate, and 3,6-endoxo-4-tetrahydrophthalate monophenyl esters, *J. Am. Chem. Soc. 118*, 2595−2605, (b) Lightstone, F. C., and Bruice, T. C. (1999) Ground state and transition state contributions to the rates of intramolecular and enzymatic reactions, *Acc. Chem. Res. 32*, 127−136, (c) Bruice, T. C., and Benkovic, S. J. (2000) Chemical basis for enzyme catalysis, *Biochemistry 39*, 6267−6274, (d) Bruice, T. C. (2002) A view at the millennium: the efficiency of enzymatic catalysis, *Acc. Chem. Res. 35*, 139−148.
47. (a) Hibbert, F., and Emsley, J. (1990) Hydrogen bonding and chemical reactivity, *Adv. Phys. Org. Chem. 26*, 255−279, (b) *Periodic Table of the Elements*, (1997) Wiley-VCH, Weinheim, Germany.
48. (a) Schulz, G. E., and Schirmer, R. H. (1979) *Principles of Protein Structure*, pp 34−36, Springer-Verlag, New York, (b) Friesner, R. A., Banks, J. L., Murphy, R. B., Halgren, T. A., Klicic, J. J., Mainz, D. T., Papasky, M. P., Knoll, E. H., Shelley, M., Perry, J. K., Shaw, D. E., Francis, P., and Shenkin, P. S. (2004) Glide: A new approach for rapid, accurate docking and scoring. 1. Method and assessment of docking accuracy, *J. Med. Chem. 47*, 1739−1749, (c) Steiner, T. (2002) The hydrogen bond in the solid state, *Angew. Chem., Int. Ed. 41*, 48−76.
49. (a) *gOpenMol*, version 2.20, Espoo, Finland, 2003. (b) Laaksonen, L. (1992) A graphics program for the analysis and display of molecular dynamics trajectories, *J. Mol. Graphics 10*, 33−34, (c) Bergman, D. L., Laaksonen, L., Laaksonen, A. (1997) Visualization of solvation structures in liquid mixtures, *J. Mol. Graphics Modell. 15*, 301−306.
50. (a) UCSF Chimera Home Page, http://www.cgl.ucsf.edu/chimera, (b) Pettersen, E. F., Goddard, T. D., Huang, C. C., Couch, G. S., Greenblatt, D. M., Meng, A. C., and Ferrin, T. E. (2004) UCSF Chimera−A visualization system for exploratory research and analysis, *J. Comput. Chem. 25*, 1605−1612.
51. Brooks, C. L., III, Karplus, M., and Pettitt, B. M. (1988) *Proteins: A Theoretical Perspective of Dynamics, Structure, and Thermodynamics*, Wiley-Interscience, New York.
52. Pletcher, J., and Sax, M. (1975) Crystal and molecular structure of thiamine pyrophosphare hydrochloride, *J. Am. Chem. Soc. 94*, 3998−4005.
53. (a) Cui, Q., Elstner, M., and Karplus, M. (2002) A Theoretical analysis of the proton and hydride transfer in liver alcohol dehydrogenase (LADH), *J. Phys. Chem. B 106*, 2721−2740, (b) Cui, Q., Karplus, M. (2003) Is a "proton wire" concerted or stepwise? A model study of proton transfer in carbonic anhydrase, *J. Phys. Chem. B 106*, 1071−1078.
54. Chang, A. K., Nixon, P. F., and Duggleby, R. G. (1999) *Zymomonas mobilis* pyruvate decarboxylase mutants, *Biochem. J. 339*, 255−260.
55. Schütz, A., Golbik, R., König, S., Hübner, G., and Tittmann, K. (2005) Intermediates and transition states in thiamine diphosphate-dependent decarboxylases. A kinetic and NMR study on wild-type indolepyruvate decarboxylase and variants using indolepyruvate, benzoylformate and pyruvate as substrates, *Biochemistry 44*, 6164−6179.
56. Clayden, J., Greeves, N., Warren, S., and Wothers, P. (2001) *Organic Chemistry*, p 200, Oxford University Press, Oxford, U.K.
57. Smith, M. B., and March, (2001) *J. March's Advanced Organic Chemistry: Reactions, Mechanisms, and Structure*, 5th ed., p 330, John Wiley & Sons, Inc., New York.
58. (a) Tittman, K, Golbik, R., Uhleman, K., Khailova, G., Patel, M., Jordan, F., Chipman, D. M., Duggleby, R. G., and Hübner, G. (2003) NMR analysis of covalent intermediates in thiamin diphosphate enzymes, *Biochemistry 42*, 7885−7891, (b) Schütz, A. Golbik, R., König, S., Hübner, G., Tittmann, K. (2005) Intermediates and transition states in thiamin diphosphate-dependent decarboxylases. A kinetic and NMR study on wild-type indolepyruvate decarboxylase and variants using indolepyruvate, bonzoylformate and pyruvate as substrates, *Biochemistry 44*, 6164−6179.
59. (a) Bürgi, H. B., Dünitz, J. D., and Shefter, E. (1973) Geometrical reaction coordinates. II. Nucleophilic addition to a carbonyl group, *J. Am. Chem. Soc. 95*, 5065−5067, (b) Bürgi, H. B., Lehn, J. M., Wipff, G. (1974) Ab initio study of nucleophilic addition to a carbonyl group, *J. Am. Chem. Soc. 96*, 1956−1957.
60. (a) Dewar, M. J. S., and Storch, D. M. (1985) Alternative view of enzyme-reactions, *Proc. Natl. Acad. Sci. U.S.A.* 82, 2225−2229. (b) Jencks, W. P. (1975) *Advances in Enzymology and Related Areas of Molecular Biology* (Meister, A., Ed.) Vol. 43, J. Wiley & Sons, Inc., New York. (c) Menger, F. (1992) Analysis of ground-state and transition-state effects on enzyme catalysis, *Biochemistry 31*, 5368−5373. (d) Menger, F. (1993) Enzyme reactivity from an organic perspective, *Acc. Chem. Res. 26*, 206−212.
61. Amara, P., Field, M. P., Alhambra, C., and Gao, J. (2000) The generalized hybrid orbital method for combined quantum mechan-

ichal/molecular mechanical calculations: formulation and tests of the analytical derivatives, *Theor. Chem. Acc. 104*, 336−343.

62. Fiedler, E., Thorell, S., Sandalova, T., Golbik, R., König, S., Schneider, G. (2002) Snapshot of a key intermediate in enzymatic thiamin catalysis: Crystal structure of the α-carbanion of (α,*β*-dihydroxylethyl)-thiamin diphosphate in the active site of transketolase from *Saccharomyces cerevisae*, *Proc. Natl. Acad. Sci. U.S.A. 99*, 591−595.
63. Nakai, T., Nakagawa, N., Maoka, N., Masui, R., Kuramitsu, S., Kamiya, N. (2004) Ligand-induced conformational changes and a reaction intermediate in branched-chain 2-oxo acid dehydrogenase (E1) from *Thermus thermophilus* HB8, as revealed by X-ray crystallography, *J. Mol. Biol. 337*, 1011−1033.
64. (a) Kato-Toma, Y., Iwashita, T., Masuda, Y., Oyama, Y., and Ishiguro, M. (2003) pK_a measurements from nuclear magnetic resonance of tyrosine-150 in class C *β*-lactamase, *Biochem. J. 371*, 175−181, (b) Shaffer, W. A., Luong, T. N., Rothman, S. C, and Kirsch, J. F (2002) Quantitative chimeric analysis of six specificity determinants that differentiate *Escherichia coli* aspartate from tyrosine aminotransferase, *Protein Sci. 11*, 2848−2859.
65. Frank, R. A. W., Titman, C. M., Pratap, J. V., Luisi, B. F., and Perham, R. N. (2004) A molecular switch and proton wire synchronize the active sites in thiamine enzymes, *Science 306*, 872−876.

BI051134Y